Spatiotemporal history of fluid-fault interaction in the Hurricane fault zone, western USA

Jace M. Koger[1] and Dennis L. Newell[1]

5   [1]Department of Geosciences, Utah State University, Logan, UT 84322, USA

Correspondence to: Dennis L. Newell (dennis.newell@usu.edu)

Abstract. The Hurricane Fault is a ~250-km-long, west-dipping normal fault located along the transition between the Colorado Plateau and Basin and Range tectonic provinces in the western U.S. Extensive evidence of fluid-fault interaction, including calcite mineralization and veining, occur in the footwall damage zone. Calcite vein carbon

10   ($\delta^{13}C_{VPDB}$) and oxygen ($\delta^{18}O_{VPDB}$) stable isotope ratios range from -4.5 to 3.8 ‰ and -22.1 to -1.1 ‰, respectively. Fluid inclusion microthermometry constrain paleofluid temperatures and salinities from 45–160 °C and 1.4–11.0 wt % as NaCl, respectively. These data identify mixing between two primary fluid sources including infiltrating meteoric groundwater (70 ± 10 °C ,~1.5 wt % NaCl, $\delta^{18}O_{SMOW}$ ~-10 ‰) and sedimentary brine (100 ± 25 °C, ~11 wt % NaCl, $\delta^{18}O_{SMOW}$ ~5 ‰). Interpreted carbon sources include crustal- or magmatic-derived CO_2, carbonate bedrock, and

15   hydrocarbons. U-Th dates from 5 calcite vein samples indicates punctuated fluid-flow and fracture healing at 539 ± 10.8, 287.9 ± 5.8, 86.2 ± 1.7, and 86.0 ± 0.2 ka in the upper 300 m of the crust. Collectively, the data imply that the Hurricane Fault imparts a strong influence on regional flow of crustal fluids, and that the formation of veins in the shallow parts of the fault damage zone has important implications for the evolution of fault strength and permeability.

1 Introduction

20   Secondary mineralization, alteration products, and associated textures in fault rocks provide windows into the history of past fluid–fault interaction in the crust. The fracture networks and associated sealing cements associated faults are widely recognized not only for their tectonic significance, but also for their impact on fluid movement and distribution in the crust of groundwater, hydrocarbons, and ore-deposits (Mozley and Goodwin, 1995; Benedicto et al., 2008; Caine and Minor, 2009; Eichhubl et al., 2009; Caine et al., 2010; Cao et al., 2010; Laubach et al., 2019). The rates,

25   spatiotemporal patterns, and mineralogy of fracture sealing in fault zones control fault-zone strength, the buildup of pore-pressures, location and frequency of failure events, and the overall fault system architecture through time (e.g., Caine et al., 1996). In order to constrain fluid-fault interaction during and after fault slip, we need information on the sources of fluids moving through the systems, their temperature and chemistry, and the age of fracture in-filling minerals that aid in their healing. Microscopy, geochronology, stable and radiogenic isotope geochemistry, bulk-rock

30   and micro-scale geochemistry, and fluid inclusion analysis of diagenetic products in fault zones collectively inform these processes.

Exhumed brittle faults and fault damage zones are excellent natural laboratories for interpreting the interaction between fluids and faults with implications for fault-zone permeability evolution, diagenesis, and the seismic cycle

35   (e.g., Chester et al., 1993; Caine et al., 1996; Sibson, 1996; Mozafari et al., 2015). Our research presented here is inspired by prior studies on exhumed normal faults in the western U.S. A common theme amongst these studies is the analyses of secondary carbonate cements and fracture filling veins. Carbonate mineralization is amenable to radiogenic and stable isotopic analyses, whole-rock elemental analysis, fluid inclusion work, and dating, which allows for interpretation of past fluid temperature, chemistry, sources, and timing of fluid flow in faults. For example, the

40   Moab Fault located in the northeastern Colorado Plateau is a world-class natural analog for the interplay between hydrocarbon-bearing fluid movement, and permeability evolution along a fault zone (Foxford et al., 1998). This east dipping normal fault exhibits a protracted history of fluid-fault interaction including hydrocarbon residues, and carbonate, oxide, and siliceous diagenetic cements and veins associated with deformation features. A suite of prior studies interprets multiple episodes fluid migration and fault-rock diagenesis between the Permian and late Tertiary

45   due to fluid expulsion from the Ancestral Rockies Paradox Basin, during Laramide deformation, and during post-Laramide extension and exhumation (Chan et al., 2000; Chan et al., 2001; Eichhubl et al., 2009; Bergman et al., 2013; Hodson et al., 2016). Also located in the Colorado Plateau, the Little Grand Wash and Salt Wash faults are well-exposed examples of carbonate-cemented normal fault zones that also serve as natural analogs for geological carbon sequestration (Shipton et al., 2004). Here extensive carbonate veins, travertine spring mounds, and CO_2-rich springs

50   and a CO_2 geyser (Crystal Geyser) are associated with normal faulting that taps a CO_2-rich fluid reservoir at depth. Fault slip, fracturing, and subsequent sealing via carbonate mineralization are interpreted to be linked to fluid pressure build-up and release. The cycle of fault slip and sealing is related to the rate of fracture filling (Frery et al., 2015), and may also be linked to changes in hydraulic head related to glacial-interglacial climatic fluctuations (Kampman et al., 2012). To the east of the Colorado Plateau, along the Rio Grande rift, exhumed basin-bounding and intra-basin normal

55   faults preserve a record of syntectonic changes to fault zone permeability due to groundwater flow and mineralization in poorly lithified siliciclastic sediments (Mozley and Goodwin, 1995; Heynekamp et al., 1999; Caine and Minor, 2009; Williams et al., 2015). These studies document progressive fluid-flow focusing along faults due to deformation and carbonate cementation that result in compartmentalization of basin hosted aquifers. Recent work on the Loma Blanca fault, in the south-central Rio Grande rift, documents periodic fault-slip and calcite sealing using microscopy,

60   isotope geochemistry, and U-Th geochronology (Williams et al., 2017a; Williams et al., 2017b; Williams et al., 2019). These studies suggest that deeply circulated, CO_2-rich fluids are focused up along this fault, and that the temporal record of calcite vein fills is linked to the earthquake cycle and fault-valve behavior in this part of the Rio Grande rift.

In this contribution, we present new results documenting paleofluid-fault interaction along the Hurricane fault-zone,

65   located at the transition between the Colorado Plateau and Basin and Range tectonic provinces of the western U.S. (Fig. 1). The Hurricane Fault is major, segmented, and seismically active normal fault located juxtaposing Mesozoic and Paleozoic sedimentary rocks along its strike, with excellent exposures of the footwall damage zone. Also proximal to and offset by the Hurricane Fault are Pliocene – Pleistocene volcanic centers and basalt flows that may have periodically altered the fluid-flow and thermal regime near the fault (Fig. 2). Prior research on the Hurricane fault has

70   focused primarily on its structural and paleoseismic history (Stewart and Taylor, 1996; Fenton et al., 2001; Lund et al., 2007), with studies on fluid-fault interaction limited to modern thermal springs (Crossey et al., 2009; Nelson et

al., 2009). We present the first quantitative results on the spatiotemporal thermochemical history of paleofluid flow and fluid-rock interaction along the Hurricane fault zone using stable isotope geochemistry, fluid-inclusion microthermometry, and U-Th geochronology of calcite vein networks exposed in the footwall damage zone.

75 Geochemical data indicate that the paleofluids migrating along the fault were mixtures of deeply circulated meteoric water and sedimentary brines with contributions from hydrocarbons and possibly recent magmatism. Textural and preliminary geochronological results from veins suggest punctuated fluid flow and fracture sealing events, possibly associated with fault slip along the Hurricane Fault.

2 Geological Setting of the Hurricane Fault

80 The Hurricane Fault strikes roughly north-south in the transition zone between the Colorado Plateau and the Basin and Range tectonic provinces in southwest Utah and northwest Arizona (Fig. 1). Major tectonic events that have shaped the region include the Sevier orogeny, Laramide orogeny, and subsequent Basin and Range extension. The Sevier orogeny and associated fold and thrust belt initiated at ~125 Ma due to subduction and formation of a continental arc along the western margin of North America (Armstrong, 1968; Heller et al., 1986). The fold and thrust

85 belt progressed eastward until shallowing of the subducting Farallon slab marked the onset of the Laramide orogeny at ca. 75 Ma (Livaccari, 1991; Yonkee and Weil, 2015). The Laramide event is marked by basement-cored uplifts and formation of the Rocky Mountains. Hydration of the continental lithosphere during this time lab led to widespread magmatism following foundering of the Farallon slab (Humphreys et al., 2003). Basin and Range extension and widespread normal faulting in the western U.S. began in the late Eocene (Axen et al., 1993).

90

Normal faults of the Basin and Range broadly follow Proterozoic accretionary and Sevier-Laramide compressional structural fabrics to accommodate late Paleogene extension (Armstrong, 1968; Quigley et al., 2002). Extension along the eastern margin of the Basin and Range adjacent to the Colorado Plateau initiated ~ 15 Ma (Axen et al., 1993). The Colorado Plateau province has remained largely un-deformed by Basin and Range extension, and the transition

95 from the thick, strong crust of the Colorado Plateau to the relatively thin crust of the Basin and Range occurs over a ~ 100-km-wide interval (Zandt et al., 1995). The eastern margin of the transition zone is also coincident with the Intermountain Seismic Belt, (Fig. 1), with multiple seismically active normal faults including the Wasatch and Hurricane fault zones (Smith et al., 1989). Late Cenozoic volcanism along the margin between the two tectonic provinces is bimodal, indicative of high heat flow and partial melting of the mantle (Best and Brimhall, 1974).

100

The Hurricane Fault is a 250-km long, segmented, west dipping normal fault in southwestern Utah and northwestern Arizona with poorly constrained origins in the mid-Miocene to Pliocene (Lund et al., 2007; Biek et al., 2010). Fault activity occurred predominantly in the Pleistocene, including up to 550 m of its total 600–850 m of vertical displacement (Lund et al., 2007). Six segments of the Hurricane Fault are 30–40 km long and have been defined based

105 on geometric and structural complexities at segmentation boundaries (Fig. S1) (Pearthree et al., 1983; Stewart and Taylor, 1996; Stenner and Pearthree, 1999). The Hurricane fault is recently active as evidenced by Quaternary scarps, and the magnitude ~5.8 earthquake occurring in 1992 east of St. George, Utah with a focus at ~15 km depth along the

projected dip of the Hurricane fault surface (Stewart and Taylor, 1996). Long-term slip rates based on paleoseismic studies range from 0.44 to 0.57 mm/y (Lund et al., 2007).

110

Rock types juxtaposed by the fault include Paleozoic and Mesozoic sandstones, siltstones and mudstones, marine limestones, and evaporites (Biek, 2003; Biek et al., 2010). Exposures of hanging wall bedrock are broadly covered by Quaternary colluvium concealing Triassic units that are exposed in a few locations. Permian and Triassic units are well exposed in the footwall along the Hurricane cliffs, especially in canyons cutting the escarpment (Fig. S2). Units

115 dominated by marine carbonates include the Permian Pakoon Dolomite, Permian Toroweap Formation, and Permian Kaibab Formation, and lower members of the Triassic Moenkopi Formation. Siliciclastic-dominated units in footwall exposures include the Permian Queantoweap Sandstone and Hermit Formation, and Triassic Moenkopi Formation. The Permian Hermit Formation includes fine-grained quartz-rich sandstones with minor hematite and calcite cements. Where exposed along the fault, the Permian Queantoweap Sandstone is composed of quartz-rich sandstone, cemented

120 by calcite and quartz.

Basaltic volcanism in the eastern Basin and Range in the transition zone to the Colorado Plateau began at ~15 Ma and has been most active within the last 2.5 My (Nelson and Tingey, 1997). Quaternary basaltic volcanic centers are spatially associated with the Hurricane fault (Fig. 2). Basalt flows are offset by the Hurricane faults, and these are

125 used for constraining long-term slip rates (Lund et al., 2007). Volcanic eruptions are predominantly alkali-rich basalts with lesser basaltic andesite. Neodymium isotope ratios of Quaternary basalts reflect primarily lithosphere sources along the northern half of the Hurricane Fault and asthenosphere/mixed source to the south (Crow et al., 2011). These periods of basaltic magmatism associated with Basin and Range extension may have created hydrothermal systems in the past that locally influenced groundwater chemistry and circulation in the Hurricane Fault.

130

Prior work on fluid movement associated with this fault is limited to geochemical and isotopic studies of modern spring systems at Pah Tempe hot spring, near La Verkin, UT, and the Travertine Grotto and Pumpkin warm springs in Grand Canyon. At Pah Tempe hot spring, deeply-circulated meteoric waters emerge as CO_2-charged and saline fluids along the fault trace, and precipitation of calcite veins is evident in the exhumed fault rocks (Nelson et al., 2009).

135 Travertine Grotto and Pumpkin warm springs are attributed to meteoric water mixing with deeply-sourced fluids that are flowing upwards along the basement-rooted Hurricane Fault (Crossey et al., 2006; Crossey et al., 2009). Analyses of volatiles exsolving from these springs identifies a predominantly deep (endogenic) source, with some modern contributions from mantle or magmatic sources.

3 Methods

3.1 Field Locations

Field investigations along the Hurricane Fault were conducted between Cedar City, UT and the fault's intersection with Grand Canyon in Arizona (Fig. 2). Studies were restricted to well-exposed areas of the fault zone, typically where drainages cross the fault. Due to colluvial cover on the hanging wall, this study focused on footwall exposures of the fault and damage zone. Twenty-three field stations (Fig. 2) along Hurricane Fault were investigated, and representative hand samples were chosen for subsequent microscopic and geochemical characterization of diagenetic alteration and secondary vein mineralization. Sampling criteria included vein morphology, cross-cutting vein relationships, varying vein/fracture orientations, and range of apparent diagenetic modification, including unaltered host rocks. Sample locations were recorded using a Garmin$_{TM}$ GPS unit in decimal degrees relative to the WGS 1984 datum (Table S1).

3.2 Microscopy

Standard petrographic thin sections were made from 34 hand samples displaying a range of vein types and diagenetic alteration. Of these 34 samples, 15 petrographic doubly polished thick sections (150 μm) of calcite veins were prepared for fluid inclusion analyses. Thin section petrographic observations were made using Leica Z16 APO and Leica DM 2700P petrographic microscopes. Photomicrograph images were acquired with a Leica MC 170 HD camera and processed using the Leica Application Suite 4.6 software.

3.3 Fluid inclusion microthermometry

Fluid inclusions in secondary calcite mineralization were investigated using a Zeiss Universal transmitted light microscope with a Zeiss Epiplan 50x long-working distance objective. A USGS gas-flow heating and freezing stage was used to measure fluid inclusion homogenization and melting temperatures. The stage was calibrated to the critical point of water using a synthetic supercritical H_2O inclusion (374.1 °C), the freezing point of a synthetic 25 mol % CO_2-H_2O inclusion (-56.6 °C), and the freezing point of double-deionized water using an ice bath (0 °C). Using the 15 thick sections, 107 homogenization temperatures (T_h) and 35 melting temperatures (T_m) were determined from two-phase fluid inclusions in calcite (Table 1).

Fluid inclusion were classified and homogenization and melting temperatures were determined using criteria and procedures described by Goldstein and Reynolds (1994) and Goldstein (2001). After performing heating measurements, numerous 2-phase fluid inclusions with homogenization temperatures from 45 – 85 °C became metastable 1-phase liquid inclusions (i.e., the bubble did not re-nucleate upon cooling). In order to re-nucleate the second phase to facilitate measuring the melting temperatures, these fluid inclusions in these samples were intentionally stretched by heating to 110 °C for 18 hours in a laboratory oven (Goldstein and Reynolds, 1994). For a few of these treated inclusions, unreliable melting temperatures >0 °C were obtained, and these were omitted from the data set. No pressure correction was performed to convert T_h measurements to trapping temperatures (T_t). Assuming vein formation at a maximum depth of 800 m equivalent to the maximum throw on the fault (Anderson and Mehnert,

1976), a maximum pressure using a lithostatic load (2675 kg m^{-3} rock density), and the maximum measured T_h of 160

175 °C, the pressure correction is <10 °C (Fisher, 1976; Bakker, 2003) and considered insignificant for this study. T_h measurements in this study are considered representative of T_t.

3.4 Carbon and oxygen stable isotope analysis

A Dremel® tool was used to collect 290 powdered sub-samples from calcite veins, mineralized fracture surfaces, limestone host rock, and calcite-cemented sandstone host rock. Carbon and oxygen stable isotope analyses of these

180 samples was performed in the Utah State University Department of Geosciences Stable Isotope Laboratory using a Thermo Scientific Delta V Advantage Isotope Ratio Mass Spectrometer (IRMS) and a GasBench II using the carbonate-phosphoric acid digestion method (McCrea, 1950; Kim et al., 2015). Specifically, ~ 120-150 µg aliquots of relatively pure calcite samples and standards were placed into 12 ml Exetainer© vials and flushed with ultra-high-purity helium. Impure carbonate cements (e.g., calcite-cemented sandstone) required 300 to 8000 µg of sample to

185 achieve acceptable peak amplitudes during analysis. After helium flushing, ~ 100 µL of anhydrous phosphoric acid was added to each sample and allowed to react for two hours at 50 °C before analysis. Carbon and oxygen stable isotope ratios were calibrated and normalized to the VPDB scale using the NBS-19 and LSVEC, and NBS-19 and NBS-18 international standards, respectively (Kim et al., 2015). In house calcite standards were used to correct for drift and mass effects. Carbon and oxygen isotope ratios are reported using delta notation (δ_{13}C, δ_{18}O) in per mil (‰)

190 relative to VPDB. Based on repeat analyses of in-house calcite standards, errors on δ_{13}C and δ_{18}O are <0.1 ‰. Oxygen isotope ratios are also converted and reported relative to standard mean ocean water (SMOW) for fluid inclusion calculations using Eq. (1) (Sharp, 2007):

$$\delta^{18}O_{SMOW} = 1.03091 * \delta^{18}O_{VPDB} + 30.91 \qquad \text{Eq. (1)}$$

3.5 Uranium-thorium (U-Th) dating

195 Pilot U-Th geochronology was conducted on 5 key calcite vein samples from two field locations (Table S2). These include locations 1-2 and 1-4, where veins are hosted in limestone and sandstone strata, respectively (Fig. 2). Veins were slabbed with a rock saw and approximately 300 mg of calcite powder was collected from discrete veins or vein laminations using a Dremel® tool and submitted to the University of Utah ICP-MS laboratory for analyses. At location 1-2, one laminated vein was subsampled at two locations (one near vein wall and near the outer part of the vein) to

200 capture the timing of vein growth. At location 1-4, 3 generations of veins, determined based on cross-cutting relationships, were subsampled.

Chemical preparation and analyses were performed at the University of Utah following methods modified from Edwards et al. (1987) using a Thermo NEPTUNE Plus Multi-Collector-Inductively-Coupled-Mass-Spectrometer

205 (MC-ICP-MS). Powdered carbonate samples were dissolved in 16 M HNO$_3$ and equilibrated with a mixed $_{229}$Th-$_{233}$U-$_{236}$U spike and refluxed on heat for at least one hour to ensure total dissolution. Uranium and thorium sample fractions were separated for analyses by anion exchange column chemistry. Measured peak heights were corrected for abundance sensitivities and mass bias, dark noise, background (blank) intensities, hydride contributions, ion-counter

yields, and spike contamination. The spike was calibrated against solutions of CRM 145 and HU1 uraninite.

210   Uncorrected age uncertainties are reported as one standard error and include measurement error and uncertainties of

activity. Details of the spike calibration and data treatment can be found in Quirk et al. (in review) .

4 Results

4.1 Fault zone diagenesis and veins

Evidence for fluid-fault interaction along Hurricane fault zone exists at the macroscopic and microscopic scale.

215   Collectively referred to as "fault zone diagenesis" (Knipe, 1992), these observations form the foundation for

subsequent geochemical and geochronological work. Examination of the fault zone at the field sites (Fig. 2) reveals

that it is composed of a ~10 to 400-m-wide damage zone, and fault core 0.5 to 2 m. The record of paleofluid flow and

deformation is best preserved in competent sandstone and limestone units within the damage zone. Evidence for

chemical and mechanical fluid-rock interaction includes host rock alteration, veins, and mineralized/cemented slip

220   surfaces, deformation bands, and breccias. Secondary minerals include primarily calcite, with lesser hematite,

manganese oxides, and gypsum. Reduction and oxidation (redox) features are observed in siltstone and sandstone

strata with calcite and iron oxide cements. Manganese and iron-oxide vein cements, and brecciated veins are primarily

observed in sandstone strata. Sparry calcite veins are the most common feature in limestone strata. The calcite veins

range from single generation mm- to cm-scale sparry fracture fills to cm-scale laminated and fibrous veins with clear

225   crystal terminations. Vein walls comprise intact host rocks (limestone and sandstone) and calcite-cemented breccia.

Diagenetic products are most commonly associated with zones of dense fracturing, although sparse veins occur

throughout the damage zone. Fracture density varies from ~2 to 20 m^{-1} within the Hurricane Fault's damage zone.

Densely fractured zones of 10–20 m^{-1} are 1–2 m wide and are pervasively mineralized and "bleached" if cutting

hematite-cemented sandstone. Fracture orientations typically follow two main sets: one striking $0 \pm 10°$ sub-parallel

230   to the fault trace, and one $300 \pm 15°$, both dipping-steeply $90 \pm 20°$. Please refer to the supplemental documentation

for more descriptions and photos of the observed veins, features associated with fault slip, and alteration of the host

rocks (Figs. S3 – S5).

4.2 Vein geochemistry

4.2.1 Carbon and Oxygen stable isotope ratios

235   Stable isotope ratios of carbon and oxygen were determined for calcite veins and host rocks from the field sites (see

data repository, Newell and Koger, 2020). The $\delta^{13}C_{VPDB}$ and $\delta^{18}O_{VPDB}$ values for the entire data set range from -4.5 to

3.8 ‰ and -22.1 to -1.1 ‰ (8.1 to 29.8 ‰ vs SMOW), respectively (Fig. 3 a). In the host rock units, carbonate cements

in siliciclastic units and bulk limestone host-rock were analysed adjacent to veins and at ~ 1–2 m away for comparison.

Host rocks near fractures have $\delta^{13}C_{VPDB}$ and $\delta^{18}O_{VPDB}$ values from -4.5 to 2.8 ‰ and -17.7 to -8.6 ‰, respectively.

240   Away from fractures, host rock $\delta^{13}C_{VPDB}$ and $\delta^{18}O_{VPDB}$ values range from -2.0 to 3.8 ‰ and -8.5 to -1.1 ‰,

respectively. The $\delta^{13}C$ and $\delta^{18}O$ values for calcite veins, breccia cements, mineralized fractures, and slip surface

cements span a wide range of values with considerable scatter. For the purposes of presentation and discussion these

data are divided into 4 "vein sets" based on common lithological associations, vein morphologic features, and $\delta_{13}C$ and $\delta_{18}O$ data patterns (Fig. 3 a). Note that these 4 vein sets span multiple locations (Fig. S1) and show no correlation

245   in C and O isotope ratios with location.

Vein set 1 calcite exhibits a positive correlation (slope = 1.6) between $\delta_{13}C$ and $\delta_{18}O$ and is commonly intergrown with hematite when hosted in siliciclastic strata. Calcite in set 2 also displays a positive $\delta_{13}C$ and $\delta_{18}O$ correlation (slope = 0.9) with $\delta_{13}C$ shifted to lower values compared to vein Set 1. Set 3 has a wide range of isotopic values,

250   showing no strong trends or patterns. Set 4 calcite $\delta_{18}O$ values that overlap with set 3 with $\delta_{13}C$ values that trend to significantly lower values. The majority of set 4 data are from location (1-2).

4.2.2 Fluid inclusion microthermometry

Of the 15 thick sections of calcite veins observed, 6 contain populations of two-phase fluid inclusions that yield homogenization (T_h) and melting (T_m) temperatures (Table 1, Fig. 4). Homogenization temperatures are used to

255   approximate the trapping temperature (T_t) and are representative of fluid temperatures during mineralization. Melting temperatures depend on the nature and concentration of dissolved species and are used to estimate the salinity of paleofluids (Bodnar, 1993).

Fluid inclusion homogenization and melting temperature data is organized by the calcite vein set as described in

260   section 4.2.1. Observed two-phase fluid inclusions range from ~5–40 μm on the long axis. Most inclusions are interpreted to be primary and there are few trails of secondary inclusions. Where present, single-phase fluid inclusion aperture is <15 μm. Homogenization temperatures for set 1 two-phase inclusions range from 45–90 °C. Vein set 3 samples have two-phase fluid inclusion homogenization temperatures from 55–160 °C, and their distribution skews towards lower temperatures, with a mode at 65–70 °C. Only small single-phase fluid inclusions are present in vein

265   sets 2 and 4. Trapping temperatures for single-phase inclusions are generally inferred as <50 °C (Goldstein and Reynolds, 1994; Goldstein, 2001). Ice melting temperatures from vein set 1 range from -3–0 °C, equating to a salinity of 0 to 5 wt% as NaCl (Fig. 4). Calcite set 3 yield melting temperatures from -11 to 0 °C, equating to 0 to 15 wt% NaCl. Since no initial melting was observed, NaCl dominated salinity is assumed and calculated via Eq. (2) where T_m is the measured melting temperature in °C (Bodnar, 1993).

270

$$(wt\% \, NaCl) = 0.00 + 1.78 \, T_m - 0.0442 \, T_m^2 + 0.000557 \, T_m^3 \qquad \text{Eq. (2)}$$

4.3 U-Th geochronology

The U-Th dates from the 5 vein samples range from 86 ka to 539 ka (Table S2). More specifically, the laminated

275   calcite vein from location 1-2, hosted in limestone strata, yields an inner lamination date of 113.1 +/- 0.3 ka and an outer lamination date of 86.2 +/- 1.7 ka (Fig. 5). The three calcite veins at location 1-4, hosted in sandstone strata yield dates of 539 +/- 10.8 ka, 287.9 +/- 5.8 ka, and 86.0 +/-0.2 ka in chronological order consistent with cross-cutting

relationships. Specifically, two dates from a single sample include calcite cement from a brecciated vein wall (288 ka) that is crosscut by a laminated calcite vein (86 ka) (Fig 5). In the field, this vein crosscuts the 539 ka vein.

280 **5 Discussion**

5.1 Paleofluid sources in the Hurricane fault

The carbon and oxygen stable isotope ratios of the calcite veins can inform the groundwater composition, source, and processes at work during paleofluid circulation in the Hurricane Fault. The C and O equilibrium isotopic fractionation between CO_2 and calcite (cc) and water and calcite (cc), respectively are temperature dependent, and assuming that

285 isotopic equilibrium during mineralization is valid, additional information on the paleofluid temperature is needed to proceed. Homogenization temperatures of primary 2-phase fluid inclusions in calcite, when present, are a reliable method to estimate temperature, and thus to calculate the paleofluid O and C isotopic composition using Eq. (3) and Eq. (4):

O isotopes: $1000ln\alpha_{H2O-cc} = 2.89 - \frac{2.78*10^6}{T^2}$ (O'Neil et al., 1969; O'Neil et al., 1975)   Eq. (3)

290

C isotopes: $1000ln\alpha_{CO2-cc} = 3.63 - \frac{1.194*10^6}{T^2}$ (Deines et al., 1974)   Eq. (4)

where α_{x-y} is the temperature dependent fractionation factor between water and calcite (H2O-cc), CO_2 and calcite (CO2-cc), and T is temperature in Kelvin. For the fractionation factor magnitudes expected for these two systems, the

295 difference in delta values between the phases (i.e., $\delta_{18}O_{H2O}$ - $\delta_{18}O_{cc}$ and $\delta_{13}C_{CO2}$ - $\delta_{13}C_{cc}$) is a good approximation for $1000ln\alpha$ (Sharp, 2007). When fluid inclusion data are not available, temperatures may be estimated based on other constraints, such as estimates on mineralization depths and the geothermal gradient, but the resulting paleofluid isotopic estimates will be far more uncertain due to surface-ward advection of geotherms (Forster and Smith, 1989). Clumped carbonate isotopic methods (Δ_{47}) can yield reliable temperature estimates from fault-zone calcite

300 mineralization (Swanson et al., 2012; Hodson et al., 2016), but are not available for this study. In the absence of these constraints, a range of temperatures or starting fluid isotopic compositions can be explored to provide some interpretations of the calcite stable isotope data, again resulting in considerable uncertainty.

For the 6 samples that hosted populations of two-phase fluid inclusions, microthermometry heating and freezing

305 data are used to estimates of fluid trapping temperatures and salinities of the paleofluids present in the Hurricane Fault. In combination with oxygen stable isotope ratios from the calcite hosting these fluid inclusions, the paleofluid $\delta^{18}O$ is calculated using Eq. (3). Although calcite oxygen stable isotope measurements are conducted on micro-drilled aliquots, these are still bulk samples when considering the microscopic distribution of fluid inclusions. Also, in each sample the microthermometry results yield populations of fluid inclusions with some variation in homogenization

310 temperature. Therefore, we cannot connect individual isotopic values to individual fluid inclusions. Rather we use the mean and standard deviation of measured temperatures in each sample along with the calcite $\delta^{18}O$ to estimate

a range of paleofluid compositions (Table 1). Similarly, we associate this range of oxygen isotope values to the mean and standard deviation of the paleofluid salinity as estimated from fluid inclusion melting temperatures. The paleofluid $\delta^{18}O$ and salinity (wt % as NaCl) estimates for these samples show a strong positive correlation (r^2 = 0.8;

315   Fig 6). We interpret this correlation as mixing between two endmember fluid types, and that over the history of fluid-fault interaction represented by these calcite veins, different proportions of ~100 +/- 25 °C, saline (~11 wt % NaCl), high $\delta^{18}O$ (~5 ‰) fluids have mixed with 70 +/- 10 °C lower salinity (~1.5 wt% NaCl), lower $\delta^{18}O$ (~-10 ‰) ground waters.

320   We suggest that the endmember characterized by high $\delta^{18}O$ and high salinity is consistent with sedimentary formation water (brine) that originated from extensive meteoric water-rock interaction and oxygen isotope exchange with marine sedimentary sequences (e.g., Clayton et al., 1966). Assuming a 25 – 30 °C geothermal gradient and the range fluid inclusion temperatures, circulation depths for these ground waters ranges from 2 to 6 km. This is adequate to infiltrate all of the Mesozoic and Paleozoic strata in the region, including thick sections of marine

325   carbonate and evaporite bearing units (Biek, 2003; Dutson, 2005; Biek et al., 2010). Infiltration into these marine units is a likely source for the salinity in these ground waters. The endmember characterized by relatively low-salinity and low $\delta^{18}O$ is likely dominantly meteoric groundwater. Using the same geothermal gradient, these ground waters have circulated to ~3.5 km based on fluid inclusion constraints. For comparison, Pah Tempe hot springs (Nelson et al., 2009), and Pumpkin and Travertine Grotto springs (Crossey et al., 2009) emanate along the Hurricane fault and

330   have similar oxygen isotope composition and salinity to this endmember (Fig. 6). Based on comparisons of Pah Tempe hot spring $\delta^{18}O$ and δ^2H with other local and regional meteoric waters, Nelson et al. (2009) interpret the source of the hot spring water as meteoric water that infiltrated during the last glacial interval. Based on geochemical geothermometry estimates, and the observed shift in hot spring water to higher $\delta^{18}O$, Nelson et al. (2009) suggest that Pah Tempe thermal waters circulation depths of 3-5 km with temperatures of 70-150 °C. This approach has also

335   been employed at other faults to interpret paleofluid compositions. For example, coupled fluid inclusion microthermometry and stable isotope values from fault-hosted calcite along the Moab fault, UT, USA, point to a mixing process between upwelling basin brines with meteorically derived groundwater (Eichhubl et al., 2009).

In terms of the carbon sources in these two fluids, there are alternative ways to interpret the relatively narrow range

340   of calcite $\delta^{13}C$ values (0.35 to 1.73 ‰). First, using the average calcite formation temperatures from fluid inclusions, we can estimate the carbon isotopic composition of the paleofluid dissolved CO_2 from -6.1 to -4.3 ‰ (VPDB) using Eq. (4) (Table 1). However, unlike the oxygen isotope system that most likely reflects the water composition, carbon composition can be reflective of a carbonate host rock. For example, dissolved carbonate in equilibrium with limestone bedrock (i.e., strongly buffered by the host rock) will result in calcite veins with a $\delta^{13}C$ similar to the host

345   limestone (e.g., Dietrich et al., 1983). In this case, calculating the carbon isotopic composition of and external CO_2 source may not be appropriate, and the vein value is simply representative of the source carbon. In this study, the

host rock limestone δ^{13}C values range from -2.7 to 3.8 ‰ with an average of 1.2 ‰, which is in the range of expected values from marine carbonates (e.g., Hoefs, 1987; Sharp, 2007). However, in parts of the fault that have higher water-rock ratios or are generally carbonate poor (e.g., siliciclastic host rock), the carbon isotopes of calcite veins

350   can be representative of an external CO_2 source dissolved and traveling in the groundwater. With these uncertainties in mind, we interpret the endmember carbon sources for the calcite veins as external CO_2 sources and local marine limestones. Based on the results from this study, there may be a weak association between the two carbon sources and the fluid endmembers based on oxygen isotopes and salinity. In some but not all cases, vein δ^{13}C values that are similar to host limestone tend to be associated with the highest salinity fluids. Veins hosted in sandstone units and

355   associated with an external CO_2 source (~-6 ‰) are in most cases associated with the lower salinity fluids. These carbon isotope values are similar to the observed δ^{13}C of CO_2 at Pah Tempe (-5.5 ‰) and Pumpkin (-6.1 ‰) springs (Crossey et al., 2009; Nelson et al., 2009). These values overlap with mantle CO_2 values (Marty and Jambon, 1987), but are also are similar to values observed in many crustal fluids and continental hot springs globally (Sherwood Lollar et al., 1997; Ballentine et al., 2002; Newell et al., 2008; Newell et al., 2015). Based on helium and carbon

360   isotopes, Crossey et al. (2009) and Nelson et al. (2009) suggest that mantle CO_2 could range from a just a few percent to as high as ~40 % in the Hurricane fault hosted hot springs, depending on the mantle and crustal endmembers used. We do not have constraints on the helium isotope ratios of the paleofluids, so we cannot further evaluate the possibility of magmatic contributions.

5.2 Subsurface processes impacting isotopic values

365   As shown earlier, the δ^{13}C and δ^{18}O values from calcite veins and cements associated with the Hurricane fault display a large range of values (Fig. 3 a). In addition to the binary mixing described in section 5.1, precipitation of calcite from fluids with a range of temperatures is occurring along flow paths. A fairly wide range of temperatures is evident from the fluid inclusion work on vein sets 1 and 3. For a given water δ^{18}O and δ^{13}C$_{CO_2}$, varying temperature in Eqs. (3) and (4) results in trends in calcite δ^{18}O and δ^{13}C with a slope of ~2.3 (Fig 3 b). To explore the impacts of both

370   temperature change and mixing, the calcite forming from the saline (δ^{18}O$_{VSMOW}$ = 5 ‰) and meteoric water (δ^{18}O$_{VSMOW}$ = -10 ‰) endmembers, both with a δ^{13}C$_{VPDB}$ = -6 ‰ are superimposed on the observed data (Fig. 3 b, shaded region). The vein set 1 pattern is fairly well matched by calcite forming over a the range of T consistent with the fluid inclusion measurements (90-45 °C) from the low-salinity meteoric end member (δ^{18}O$_{VSMOW}$ = -10 ‰ ; δ^{13}C$_{VPDB}$ = -6 ‰). The scattered values observed for vein set 3 are encompassed by the calcite forming from mixed

375   saline and meteoric fluids over the range of temperatures consistent with the fluid inclusion measurements (160-50 °C). Although not shown on the diagram, using a limestone-buffered δ^{13}C (~1 ‰) predicts values that are *not* consistent with any of the observed data, and this suggests that an external source of CO_2 may be most appropriate for veins in both the carbonate and siliciclastic host rock. The vein set 4 isotopic values are best explained by mixing the saline end member at ~100 °C with a δ^{13}C source of ~ -12 ‰ (Fig. 3 b). This low δ^{13}C value is consistent with

380   derivation from organic matter (Boles et al., 2004). Hydrocarbons are present regionally and in the strata that hosts

the Hurricane fault (Bahr, 1963; Blakey, 1979). Mobilization and microbial oxidation of these hydrocarbons to form dissolved carbonate (Baedecker et al., 1993; Tuccillo et al., 1999) has been shown in other fault settings to form calcite veins with low δ^{13}C values (e.g., Eichhubl et al., 2009).

385 Open-system processes can also result in a range of calcite O and C stable isotope values. For example, open system CO_2 degassing and calcite precipitation results in progressive fractionation of C and O stable isotopes in the fluid that result in correlations between δ^{13}C and δ^{18}O values (Hendy, 1971). Kampman et al. (2012) used a Rayleigh fractionation model, assuming isotopic equilibrium, to describe C and O stable isotope values observed in fault-controlled aragonite veins and travertine deposits in the Salt Wash Graben, UT, USA. Here, coupled CO_2 degassing

390 and carbonate precipitation from a homogenous CO_2-charged fluid source can explain the positive correlation and range in δ^{13}C and δ^{18}O values. In combination with U-Th geochronological constraints, these authors suggest that this system has been active periodically for >100 ky with a consistent paleofluid source and isotopic composition.

Here we test if the positively correlated C and O values observed for vein set 1 (slope = 1.6) and set 2 (slope = 0.9)
395 (Fig 3 a) can be explained by a similar process. Rayleigh fractionation trends are included on figure 3 (b) for calcite resulting from open system CO_2 degassing (CO2-DIC), coupled CO_2 degassing and calcite precipitation (CO2-DIC-CC), and calcite precipitation from groundwater (DIC-CC). These are calculated for both the carbon and oxygen isotope system using a Rayleigh distillation approach similar to Kampman et al. (2012). For example, for the progressive formation of calcite from bicarbonate, the carbon isotope ratios can be calculated from Eq. (5):

400

$$\delta^{13}C = \delta^{13}C_o - [1000 \times ln\alpha_{product-HCO3}(1 - F)] \qquad \text{Eq. (5)}$$

where $\delta^{13}C_o$ is the starting carbon isotope ratio for HCO_3^- in solution, and F is the fraction of the C remaining in solution. Temperature dependent equilibrium fractionation factors (α) for carbon isotopes in the calcite, CO_2,
405 dissolved inorganic carbon (DIC) system are derived from Deines et al. (1974). We assume that the paleofluids were slightly acidic (~6.5) and near the equivalence point of H_2CO_3 and HCO_3^- to compute the $\alpha_{DIC-CO2}$ (Gilfillan et al., 2009). This is consistent with pH and geochemical observations at Pah Tempe hot springs and Pumpkin spring (Crossey et al., 2009; Nelson et al., 2009). Assuming the precipitation of calcite based on: $CaCO_{3(calcite)} + CO_{2(g)} + H_2O \Leftrightarrow 2HCO_3^-_{(aq)} + Ca^{2+}_{(aq)}$, the formation of calcite from HCO_3^- in solution partitions, on a molar basis, the carbon equally between
410 calcite and CO_2. Using the approach of Kampman et al. (2012), the net fractionation factor between the products and the bicarbonate in solution based on Eq. (6) is:

$$\alpha_{product-HCO3} = 1/2 (\alpha_{calcite-HCO3^-}) + 1/2(\alpha_{DIC-CO2}) \qquad \text{Eq. (6)}$$

415 Similarly, the oxygen isotope fractionation factor is calculated using Eq. (7):

$\alpha_{product-HCO3} = 1/3(\alpha_{CO2-HCO3}) + 1/2(\alpha_{calcite-HCO3}) + 1/6(\alpha_{H2O-HCO3})$ Eq. (7)

The oxygen isotope system temperature dependent fractionation factors are derived from published relationships (O'Neil et al., 1969; O'Neil et al., 1975; Beck et al., 2005).

420

Focusing on vein set 1 and a range of temperatures observed from fluid inclusion, the computed trends cannot explain the observed data (Fig. 3 b). Rayleigh fractionation trends under equilibrium conditions for CO_2 degassing and coupled CO_2 degassing + calcite precipitation <85 °C yield positive correlations that are not similar to the observed slope or range of values in set 1 calcite veins. Based on this analysis, it is unlikely that open system

425 processes such as these are major processes involved in the formation of calcite veins in the Hurricane fault zone. It is important to note that these Rayleigh fractionation models assume isotopic equilibrium. Rapid degassing and calcite precipitation may result in disequilibrium and kinetic fractionation that cannot be quantitatively addressed.

To summarize these analyses and interpretations, most of the vein C and O isotopic compositions observed can be
430 explained by a combination of the mixing of two primary fluid endmembers over a range of temperatures, with second order impacts from open system processes such as degassing during calcite precipitation. Vein set 1 is best explained by formation over a range of temperatures from the low-salinity endmember. Most of the values in set 2 and 3 can be explained by a mixture of the low-salinity meteoric and the sedimentary brine end members and precipitation over a range of temperatures. Vein set 4 requires addition of a much lower $\delta^{13}C$ component to the
435 fluids responsible for vein set 3, likely derived from an organic source.

5.3 Implications of vein geochronology

Pilot U-Th geochronology on 5 samples indicates that calcite veins formed from 539 to 86 ka. These samples are from two different sample locations (1-2 and 1-4) separated by 13 km along strike (Fig. 2, 5), and from vein sets 1, 3, and 4. Specifically, at location 1-2, hosted in limestone, veins formed at 133 ka and 86 ka (set 4). At location 1-4, hosted
440 in sandstone, veins formed at 539 and 288 ka (set 1) and 86 ka (set 3). As described in the results, the dates are consistent with interpreted vein growth direction and cross-cutting relationships (Fig. 5).

Based on the stable isotope results and analyses, the 539 and 288 ka veins are likely associated with the low-salinity meteoric water endmember (Fig. S6) and formed at moderate temperatures (60-70 °C). The 113 ka and both 86 ka
445 veins are best associated with ~100 °C saline groundwater, with varying contributions of a low $\delta_{13}C$ carbon source (Fig. S6). The 86 ka sample from location 1-2 has the lowest $\delta_{13}C$ (-7 ‰) observed in this study, and as discussed in section 5.2 requires an organic carbon source.

Although this data set is small, it suggests punctuated vein forming events. Interestingly, these two fault locations
450 appear to preserve the 86 ka event, both requiring similar composition and temperature fluids, suggesting that the fluid

circulation events have continuity over ~13 km of fault zone strike. These dates can be used along with constraints on fault slip rate to estimate the maximum depth of vein formation. Using the published slip rate estimates of 0.44 to 0.57 mm/y (Lund et al., 2007), this equates to vein formation of depths of ~40 to 300 m. This assumes negligible exhumation of the footwall over the last 540 ka. Consistent with the findings at thermal springs along the Hurricane

455 Fault (Crossey et al., 2006; Crossey et al., 2009; Nelson et al., 2009), this indicates that deeply-circulated thermal fluids are moving up the fault zone, advecting deeper geotherms towards the surface.

Although not the primary objective of this paper, the calcite vein textures in context of the preliminary geochronological results warrant a brief discussion. The vein wall breccias and laminated calcite veins observed along

460 the Hurricane Fault share similar characteristics to those in other major fault zones that have been attributed to co-seismic or post-seismic sealing (e.g., Nuriel et al., 2011; Nuriel et al., 2012). These fracture openings filled with laminated growth bands of fibrous calcite crystal are indicative of post-fracture opening sealing (crack-seal cycle) (Ramsay, 1980). These suggest fluid-pressurization and fluid flow cycles associated with periodic fracturing in the fault damage zone, possibly due to seismic activity (e.g., Sibson, 1994). Williams et al. (2017b) showed that detailed

465 U-Th dating of these types of laminated veins inform the periodic nature of fracture opening and sealing via calcite precipitation and argue these are associated with seismic events. Specifically, they documented 13 seismic events between 550 ka and 150 ka and use this to estimate long-term earthquake recurrence intervals. In addition to earthquakes, Pleistocene climatic cycles could influence groundwater flow and fluid pressure, and possibly be associated with vein forming events similar to what is observed at the Little Grand Wash and Salt Wash faults (e.g.,

470 Kampman et al., 2012). We have documented 4 such events in the last ~540 ka, suggesting that a similar high-resolution geochronological study could yield meaningful information about the long-term recurrence of fluid-flow triggering events along the Hurricane fault zone, whether triggered by seismicity or linked to climatic cycles.

6 Summary and Conclusions

Integrated calcite vein stable isotope geochemistry, fluid inclusion microthermometry and U-Th geochronology

475 document the nature of paleofluids circulating in the Hurricane Fault over the last ~540 ky. Our results indicate that calcite veins form in the footwall damage zone of the fault from mixtures of two main fluids over a range of temperatures. These include a relatively low salinity meteoric-affinity groundwater and a salty sedimentary formation water. Carbon sources are more ambiguous, but likely include significant contributions from crustal or magmatic CO_2 and carbonate bedrock, along with lesser amounts from hydrocarbons. Fluid inclusion microthermometry temperatures

480 from ~45 to 160 °C indicating that these fluids have circulated deeply (up to 6 km) prior to flowing up the Hurricane fault zone. Our pilot geochronology is sparse (5 dates) but supports punctuated vein forming events at 539, 289, 113, and 86 ka. Considering the published long-term slip rates along the Hurricane Fault, these veins likely formed in the upper 40–300 m of the crust. Present-day up flow of similar composition fluids occurs at Pah Tempe hot spring and where the fault cuts the Colorado River in Grand Canyon at Pumpkin and Travertine Grotto springs.

485

These results have implications for how the paleohydrology of the Hurricane Fault changes spatially and through time. Calcite cemented fault breccia and laminated, fibrous calcite veins are suggestive of cycles of fracture opening and healing (i.e., crack-seal textures). Deep groundwater circulation and fault processes result in high pore pressures in the fault zone, and subsequent fracturing triggers up flow of CO_2-charged thermal fluids, fluid-rock interaction in the

490 fault zone, and mixing with other ground waters. Calcite mineralization and veining from these flowing fluids heals breccias and fractures. The multiple generations of cross-cutting veins and laminated veins indicates that healed parts of the fault have experienced this cycle multiple times. Data from this study show that these linked mechanical and hydrological processes are occurring in the upper 40 – 300 m of the fault zone and is occurring periodically over ~180 km of fault strike. We conclude that the Hurricane Fault imparts a strong influence on regional flow of crustal fluids,

495 and that the formation of veins in the shallow parts of the fault damage zone has important implications for fault strength in the upper most part of the crust.

7 Data Availability

Readers are invited to access the full data set archived on the EarthChem Library: https://doi.org/10.26022/IEDA/111542. (Newell and Koger, 2020).

500 **8 Supplemental Information**

Supplemental information, tables, figures are available at the following link: XXXXXX.

9 Author Contributions

Jace Koger conducted the field sample collection, sample preparation, and sample analyses as part of the requirement for his MSc in Geology from Utah State University (Koger, 2017). Dennis Newell was the thesis supervisor, provided

505 assistance and mentorship on sampling and analytical techniques, guidance on data analysis, and is the corresponding author for the preparation of this manuscript.

10 Competing Interests

None.

11 Acknowledgements

510 We thank Andrew Lonero (USU Geosciences) and Diego Fernandez (University of Utah) for their assistance with stable isotopic and U-Th analyses, respectively. Funding for this research was provided by a Geological Society of America Student Research Grant to J. Koger and the Department of Geosciences at USU.

Tables and Figures

515

Table 1. Calculated paleofluid δ13C and δ18O from calcite C and O stable isotopes and microthermometry

Field Station	Sample ID	$\delta_{13}C_{cc}$ ‰ (VPDB)	$\delta_{18}O_{cc}$ ‰ (SMOW)	T_h (°C)	T_m (°C)	wt % NaCl$_a$	$\delta_{13}C_{CO2b}$ ‰ (VPDB)	$\delta_{18}O_{H2Oc}$ ‰ (SMOW)
1-2	JK15HR41	0.55	22.6	102.5 ± 25.0	-7.5 ± 1.7	11.0 ± 1.4	-4.3 ± 1.1	5.6 ± 2.7
1-4	JK15HR110	0.50	10.0	75.8 ± 2.3	-2.2 ± 0.9	3.7 ± 0.5	-5.7 ± 0.1	-10.0 ± 0.3
3-1	JK15HR151	1.27	9.8	66.7 ± 11.0	-0.8 ± 0.3	1.4 ± 0.6	-5.4 ± 0.7	-11.4 ± 1.5
3-4	JK15HR160	0.35	20.2	71.6 ± 9.8	-3.2 ± 1.2	5.2 ± 1.8	-6.1 ± 0.6	-0.5 ± 1.3
3-5	JK15HR169	0.77	18.3	72.2 ± 8.7	-2.0 ± 1.9	4.7 ± 2.6	-5.6 ± 0.5	-2.3 ± 1.2
5-2	JK15HR255	1.73	13.5	70.1 ± 7.0	-1.0 ± 0.2	1.7 ± 0.7	-4.8 ± 0.4	-7.2 ± 1.0
-	Pah Tempe HS$_d$	-	-	-	-	0.8	-5.5	-13.0
-	Pumpkin Spr$_e$	-	-	-	-	1.1	-6.1	-10.6
	Travertine Grotto$_e$	-	-	-	-	0.2	-	-10.8

$_{a,b,c}$ calculated using Eq. (2), (4), and (3), respectively
$_d$Nelson et al. (2004); $_e$Crossey et al. (2009)
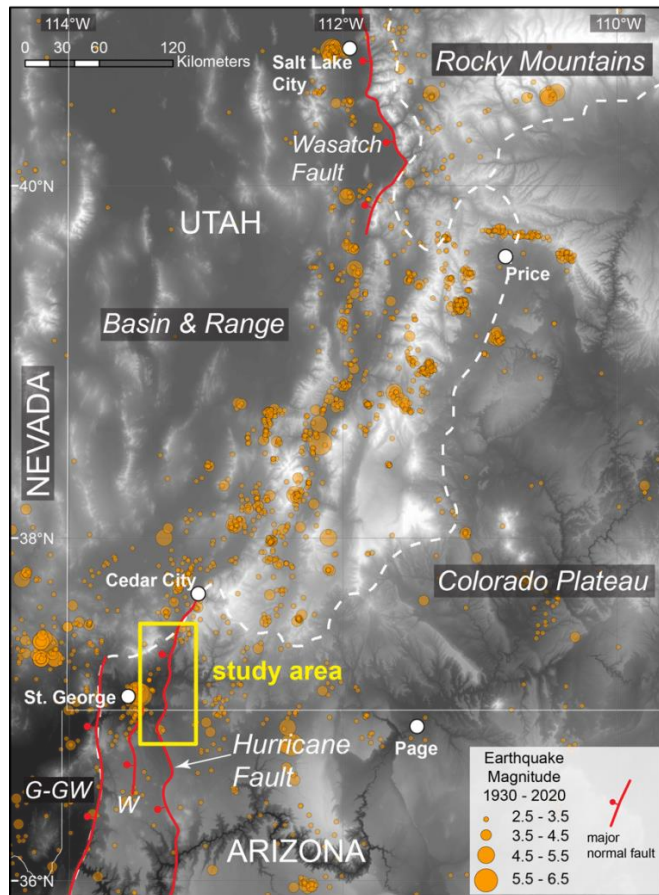
Figure 1: Location of the Hurricane Fault and study area along the boundary between the Colorado Plateau and Basin and Range tectonic provinces in the western U.S. The fault is located within the Intermountain Seismic belt as delineated by the depicted >M 2.5 earthquakes from 1930 – 2020 (USGS, 2020). Other notable faults in the region include the Gunlock-Grand Wash (G-GW) and Wasatch faults. (Digital Elevation, SRTM 1 Arc-Second Global 10.5066/F7PR7TFT, courtesy of the U.S. Geological Survey)

520

525
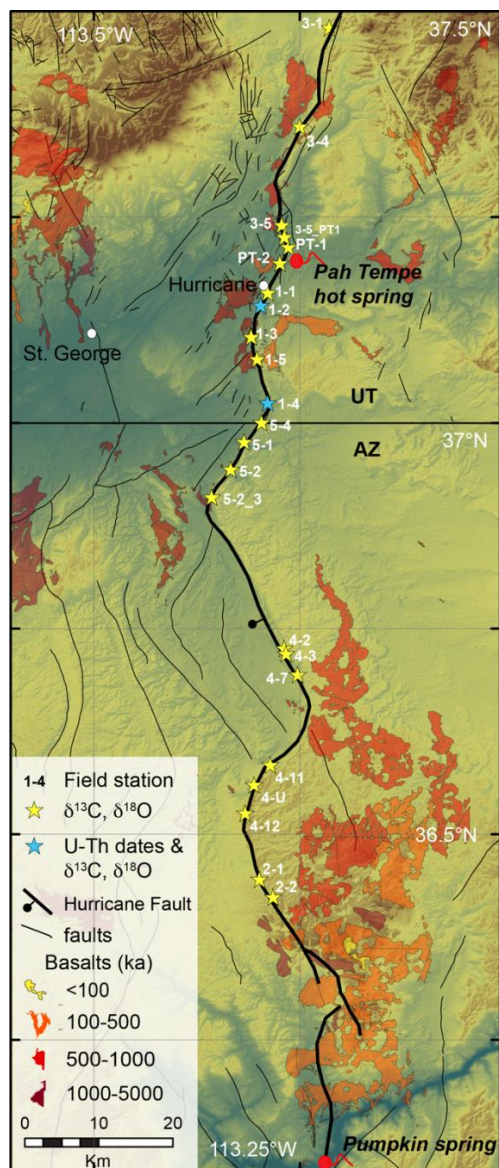
Figure 2: The Hurricane Fault extent in southern Utah and northern Arizona with the 23 Field Stations investigated in this study. Note that C and O isotope values from calcite veins are reported for all field sites. Additionally, U-Th dates are reported from stations 1-2 and 1-4. Locations of Pah Tempe and Pumpkin springs are shown. Travertine Grotto is located south of map extent.
530   Geology from (Billingsley and Workman, 2000; Billingsley and Wellmeyer, 2003; Rowley et al., 2008). (Digital Elevation, SRTM 1 Arc-Second Global 10.5066/F7PR7TFT, courtesy of the U.S. Geological Survey)
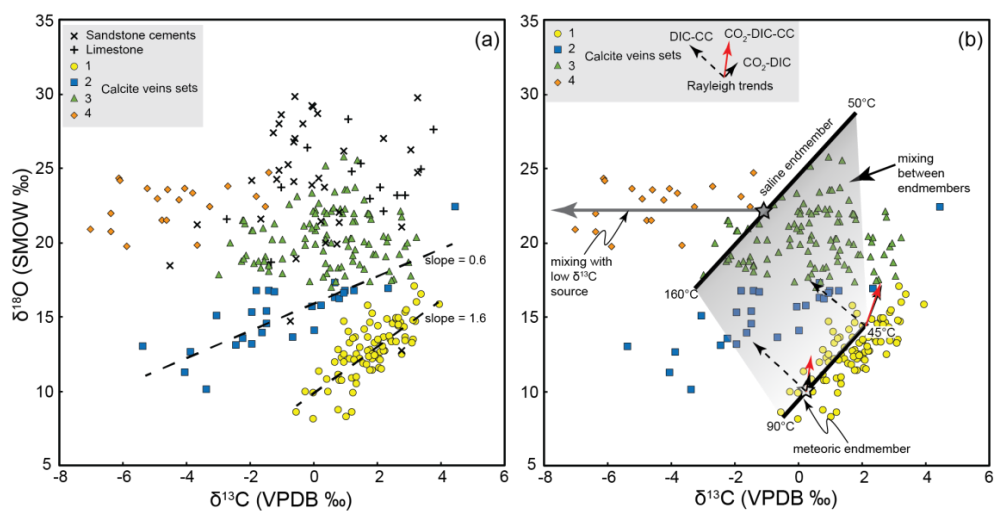
Figure 3. (a) Calcite oxygen and carbon stable isotope values for veins and host rocks along the Hurricane Fault. Host rock values are from bulk limestone samples and from calcite cemented sandstones. The veins are divided into 4 veins sets for analysis. Note the trend line slopes for vein sets 1 and 2 **(b)** Paleofluid interpretations integrating the isotopic and fluid inclusion microthermometry results. Mixing scenarios depicted include the mixing of two endmember fluids over a range of temperature and the mixing with a low $\delta^{13}C$ CO_2 source. Also shown are the open-system Rayleigh fractionation trends due progressive precipitation of calcite from water dissolved inorganic carbon (DIC-CC), progressive CO_2 loss from the water dissolved inorganic carbon (CO2-DIC), and the combined effects of CO2 degassing and calcite precipitation (CO2-DIC-CC).
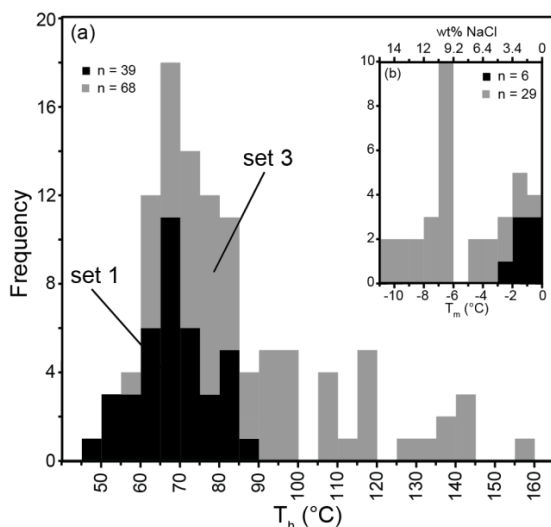
545

Figure 4: (a) Fluid inclusion (2-phase) homogenization temperatures from vein set 1 and 3. **(b)** Fluid inclusion melting temperatures from vein sets 1 and 3 and the calculated salinity as wt% NaCl (see text for details).
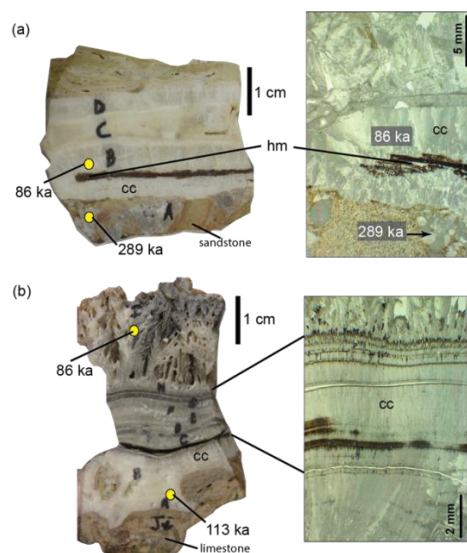
550   **Figure 5: (a)** Laminated calcite vein from location 1-4 and associated U-Th dates (samples JK15HR110 and JK15HR111). Hand specimen (left) and plane-polarized photomicrograph (right) shown. Note the calcite cemented brecciated sandstone forming the vein wall. The laminated calcite vein shows at least 4 episodes of calcite precipitation. The calcite cement in the wall breccia is 289 ka and the first lamination growing on the vein wall is 86 ka. **(b)** Laminated calcite vein from location 1-2 that is hosted in marine limestone. U-Th dates (JK15HR27 and JK15HR35) are shown on the hand specimen. The dates indicate growth outward from the
555   limestone wall from 113 ka to 86 ka. Multiple dense laminations are visible in hand sample, and the plane polarized photomicrograph shows these are constructed of fibrous calcite crystals that terminate at discrete boundaries. The outermost (86 ka) layer is characterized by higher porosity vuggy calcite crystals suggestive of growth into free fluids.
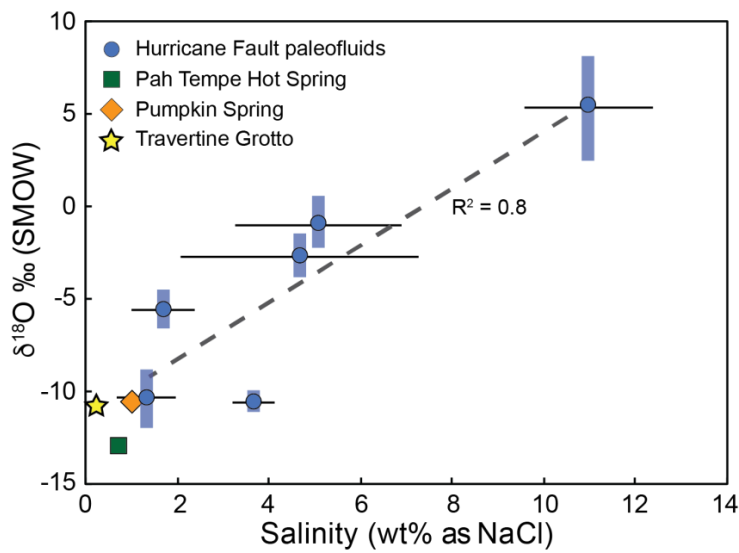
Figure 6. Calculated paleofluid oxygen isotope composition versus fluid salinity determined by fluid inclusion microthermometry. The strong positive correlation of $\delta_{18}O$ and salinity ($R_2 = 0.8$) is interpreted as a mixing trend between and low salinity, meteoric-affinity groundwater and high salinity sedimentary brine endmember. For comparison, the composition of Pah Tempe, Pumpkin, and Travertine Grotto springs are included, are very similar in composition to the low salinity endmember.

565 **References**

Anderson, R. E., and Mehnert, H. H.: Reinterpretation of the history of the Hurricane fault in Utah, in: Basin and Range Conference Guidebook: Geological Society of Nevada, Rocky Mountain Association of Geologists, and Utah Geological Society, edited by: Newman, G. W., 145-165, 1976.

Armstrong, R. L.: Sevier orogenic belt in Nevada and Utah, Geological Society of America Bulletin, 79, 429-458, 1968.

570 Axen, G. J., Taylor, W. J., and Bartley, J. M.: Space-time patterns and tectonic controls of Tertiary extension and magmatism in the Great Basin of the western United States, Geological Society of America Bulletin, 105, 56-76, 1993.

Baedecker, M. J., Cozzarelli, I. M., Eganhouse, R. P., Siegel, D. I., and Bennett, P. C.: Crude oil in a shallow sand and gravel aquifer—III. Biogeochemical reactions and mass balance modeling in anoxic groundwater, Applied Geochemistry, 8, 569-586, 1993.

575 Bahr, C. W.: Virgin oil field, Washington County, Utah, in: Guidbook to the geology of southwestern Utah: Transition between basin-range and Colorado plateau provinces, edited by: Heylmun, E. B., Intermountain Association of Petroleum Geologists, Salt Lake City, 169 - 171, 1963.

Bakker, R. J.: Package FLUIDS 1. Computer programs for analysis of fluid inclusion data and for modelling bulk fluid properties, Chemical Geology, 194, 3-23, 2003.

580 Ballentine, C. J., Burgess, R., and Marty, B.: Tracing Fluid Origin, Transport and Interaction in the Crust, in: Reviews in Mineralogy & Geochemistry - Noble Gases in Geochemistry and Cosmochemistry, edited by: Porcelli, D., Ballentine, C. J., and Wieler, R., Mineralogical Society of America, Washington D.C., 539-614, 2002.

Beck, W. C., Grossman, E. L., and Morse, J. W.: Experimental studies of oxygen isotope fractionation in the carbonic acid system at 15, 25, and 40 C, Geochimica et Cosmochimica Acta, 69, 3493-3503, 2005.

585 Benedicto, A., Plagnes, A., Vergely, P., Flotte, N., and Schultz, R. A.: Fault and fluid interaction in a rifted margin: integrated study of calcite-sealed fault-related structures (southern Corinth margin), in: The Internal Structure of Fault Zones: Implications for Mechanical and Fluid-Flow Properties, edited by: Wibberley, C. A. J., Kurz, W., Imber, J., Holdsworth, R. E., and Collettini, C., Geological Society of London, 257-275, 2008.

Bergman, S., Huntington, K. W., and Crider, J. G.: Tracing paleofluid sources using clumped isotope thermometry of diagenetic
590 cements along the Moab Fault, Utah, American Journal of Science, 313, 490-515, 2013.

Best, M., and Brimhall, W.: Late Cenozoic alkalic basaltic magmas in the western Colorado Plateaus and the Basin and Range transition zone, USA, and their bearing on mantle dynamics, Geological Society of America Bulletin, 85, 1677-1690, 1974.

Biek, R.: Geologic Map of the Hurricane Quadrangle Washington County, Utah: Utah Geological Survey Map, 187, 2003.

Biek, R., Rowley, P., Hayden, J., Hacker, D., Willis, G., Hintze, L., Anderson, R., and Brown, K.: Geologic map of the St. George
595 and east part of the Clover Mountains 30'X60' quadrangles, Washington and Iron counties, Utah, Utah Geological Society, 2010.

Billingsley, G., and Workman, J.: Geological map of the Littlefield 30' X 60' quadrangle, Mohave County, northwestern Arizona, U.S.G.S, 2000.

Billingsley, G., and Wellmeyer, J.: Geologic map of the Mount Trumbull 30' X 60' quadrangle, Mohave and Coconino Counties, northwestern Arizona, U.S.G.S., 2003.

600 Blakey, R.: Oil impregnated carbonate rocks of the Timpoweap Member Moenkopi Formation, Hurricane Cliffs area, Utah and Arizona, Utah Geology, 6, 45-54, 1979.

Bodnar, R. J.: Revised equation and table for determining the freezing point depression of H2O-NaCl solutions, Geochimica et Cosmochimica Acta, 57, 683-684, 1993.

Boles, J. R., Eichhubl, P., Garven, G., and Chen, J.: Evolution of a hydrocarbon migration pathway along basin-bounding faults:
605 Evidence from fault cement, AAPG bulletin, 88, 947-970, 2004.

Caine, J. S., Evans, J. P., and Forster, C. B.: Fault zone architecture and permeability structure, Geology, 24, 1025-1028, 1996.

Caine, J. S., and Minor, S. A.: Structural and geochemical characteristics of faulted sediments and inferences on the role of water in deformation, Rio Grande Rift, New Mexico, Geological Society of America Bulletin, 121, 1325-1340, 2009.

Caine, J. S., Bruhn, R. L., and Forster, C. B.: Internal structure, fault rocks, and inferences regarding deformation, fluid flow, and mineralization in the seismogenic Stillwater normal fault, Dixie Valley, Nevada, Journal of Structural Geology, 32, 1576-1589, 2010.

Cao, J., Jin, Z., Hu, W., Zhang, Y., Yao, S., Wang, X., Zhang, Y., and Tang, Y.: Improved understanding of petroleum migration history in the Hongche fault zone, northwestern Junggar Basin (northwest China): Constrained by vein-calcite fluid inclusions and trace elements, Marine and Petroleum Geology, 27, 61-68, 2010.

Chan, M. A., Parry, W., and Bowman, J.: Diagenetic hematite and manganese oxides and fault-related fluid flow in Jurassic sandstones, southeastern Utah, AAPG bulletin, 84, 1281-1310, 2000.

Chan, M. A., Parry, W. T., Petersen, E. U., and Hall, C. M.: 40Ar/39Ar age and chemistry of manganese mineralization in the Moab and Lisbon fault systems, southeastern Utah, Geology, 29, 331-334, 2001.

Chester, F. M., Evans, J. P., and Biegel, R. L.: Internal structure and weakening mechanisms of the San Andreas fault, Journal of Geophysical Research: Solid Earth, 98, 771-786, 1993.

Clayton, R. N., Friedman, I., Graf, D. L., Mayeda, T. K., Meents, W. F., and Shimp, N. F.: The origin of saline formation waters, I: Isotopic composition, Journal of Geophysical Research, 71, 3869-3882, 1966.

Crossey, L. J., Fischer, T. P., Patchett, P. J., Karlstrom, K. E., Hilton, D. R., Huntoon, P., Newell, D., and Reynolds, A.: Dissected hydrologic system at the Grand Canyon: Interaction between deeply derived fluids and plateau aquifer waters in modern springs and travertine, Geology, 34, 25-28, 2006.

Crossey, L. J., Karlstrom, K. E., Springer, A., Newell, D. L., Hilton, D. R., and Fischer, T. P.: Degassing of mantle-derived CO_2 and ^3He from springs in the southern Colorado Plateau region - flux rates, neotectonic connections, and implications for groundwater systems, GSA Bulletin, 21, 1034 - 1053, 2009.

Crow, R., Karlstrom, K., Asmerom, Y., Schmandt, B., Polyak, V., and DuFrane, S. A.: Shrinking of the Colorado Plateau via lithospheric mantle erosion: Evidence from Nd and Sr isotopes and geochronology of Neogene basalts, Geology, 39, 27-30, 2011.

Deines, P., Langmuir, D., and Harmon, R. S.: Stable carbon isotope ratios and the existence of a gas phase in the evolution of carbonate ground waters, Geochimica et Cosmochimica Acta, 38, 1147-1164, 1974.

Dietrich, D., McKenzie, J. A., and Song, H.: Origin of calcite in syntectonic veins as determined from carbon-isotope ratios, Geology, 11, 547-551, 10.1130/0091-7613(1983)11<547:OOCISV>2.0.CO;2, 1983.

Dutson, S.: Effects of Hurricane Fault Architecture on Groundwater Flow in the Timpoweap Canyon of Southwestern, Utah [MS thesis]: Provo, Brigham Young University, 2005.

Edwards, R. L., Chen, J. H., and Wasserburg, G.: ^{238}U-^{234}U-^{230}Th-^{232}Th systematics and the precise measurement of time over the past 500,000 years, Earth and Planetary Science Letters, 81, 175-192, 1987.

Eichhubl, P., Davatzes, N. C., and Becker, S. P.: Structural and diagenetic control of fluid migration and cementation along the Moab fault, Utah, AAPG Bulletin, 93, 653-681, 2009.

Fenton, C. R., Webb, R. H., Pearthree, P. A., Cerline, T. E., and Poreda, R. J.: Displacement rates on the Toroweap and Hurricane faults: Implications for Quaternary downcutting in the Grand Canyon, Arizona, Geology, 29, 1035 - 1038, 2001.

Fisher, J. R.: The volumetric properties of H_2O, J. Res. Us. Geol. Survey, 4, 189-193, 1976.

Forster, C. B., and Smith, L.: The influence of groundwater flow on thermal regimes in mountainous terrain: A model study, Journal of Geophysical Research, 94, 9439-9451, 1989.

Foxford, K., Walsh, J., Watterson, J., Garden, I. R., Guscott, S., and Burley, S.: Structure and content of the Moab Fault Zone, Utah, USA, and its implications for fault seal prediction, Geological Society, London, Special Publications, 147, 87-103, 1998.

Frery, E., Gratier, J.-P., Ellouz-Zimmerman, N., Loiselet, C., Braun, J., Deschamps, P., Blamart, D., Hamelin, B., and Sennen, R.: Evolution of fault permeability during episodic fluid circulation: Evidence for the effects fo fluid-rock interactions from travertine
650 studies (Utah-USA), Tectonophysics, 651-652, 121-137, 2015.

Gilfillan, S. M. V., Sherwood Lollar, B., Holland, G., Blagburn, D., Stevens, S., Schoell, M., Cassidy, M., Ding, Z., Zhou, Z., Lacrampe-Couloume, G., and Ballentine, C. J.: Solubility trapping in formation water as dominant CO_2 sink in natural gas fields, Nature, 458, 614-617, 2009.

Goldstein, R. H., and Reynolds, T. J.: Systematics of fluid inclusions in diagenetic minerals/ SEPM Short Course 31, Tulsa, OK,
655 199 pp., 1994.

Goldstein, R. H.: Fluid inclusions in sedimentary and diagenetic systems, Lithos, 55, 159-193, 2001.

Heller, P., Bowdler, S., Chambers, H., Coogan, J., Hagen, E., Shuster, M., Winslow, N., and Lawton, T.: Time of initial thrusting in the Sevier orogenic belt, Idaho-Wyoming and Utah, Geology, 14, 388-391, 1986.

Hendy, C. H.: The isotopic geochemistry of speleothems—I. The calculation of the effects of different modes of formation on the
660 isotopic composition of speleothems and their applicability as palaeoclimatic indicators, Geochimica et cosmochimica Acta, 35, 801-824, 1971.

Heynekamp, M. R., Goodwin, L. B., Mozley, P. S., and Haneberg, W. C.: Controls on fault-zone architecture in poorly lithified sediments, Rio Grande Rift, New Mexico: Implications for fault-zone permeability and fluid flow, Washington DC American Geophysical Union Geophysical Monograph Series, 113, 27-49, 1999.

665 Hodson, K. R., Crider, J. G., and Huntington, K. W.: Temperature and composition of carbonate cements record early structural control on cementation in a nascent deformation band fault zone: Moab Fault, Utah, USA, Tectonophysics, 690, 240-252, 2016.

Hoefs, J.: Stable Isotope Geochemistry, 3 ed., Springer-Verlag, New York, 241 pp., 1987.

Humphreys, E., Hessler, E., Dueker, K., Farmer, G. L., Erslev, E., and Atwater, T.: How Laramide-age hydration of North American lithosphere by the Farallon Slab controlled subsequent activity in the Western United States, International Geology Review, 45,
670 575-595, 2003.

Kampman, N., Burnside, N. M., Shipton, Z. K., Chapman, H. J., Nicholl, J. A., Ellam, R. M., and Bickle, M. J.: Pulses of carbon dioxide emissions from intracrustal faults following climatic warming, Nature Geoscience, 5, 352-358, 2012.

Kim, S.-T., Coplen, T. B., and Horita, J.: Normalization of stable isotope data for carbonate minerals: Implementation of IUPAC guidelines, Geochimica et Cosmochimica Acta, 158, 276 - 289, 2015.

675 Knipe, R.: Faulting processes and fault seal, in: Structural and tectonic modelling and its application to petroleum geology, Elsevier, 325-342, 1992.

Koger, J. M.: Spatio-Temporal History of Fluid-Rock Interaction in the Hurricane Fault Zone, MS, Utah State University, 158 pp., 2017.

Laubach, S. E., Lander, R., Criscenti, L. J., Anovitz, L. M., Urai, J., Pollyea, R., Hooker, J. N., Narr, W., Evans, M. A., and Kerisit,
680 S. N.: The role of chemistry in fracture pattern development and opportunities to advance interpretations of geological materials, Reviews of Geophysics, 57, 1065-1111, 2019.

Livaccari, R. F.: Role of crustal thickening and extensional collapse in the tectonic evolution of the Sevier-Laramide orogeny, western United States, Geology, 19, 1104-1107, 1991.

Lund, W., Hozik, M., and Hatfield, S.: Paleoseismic investigation and long-term slip history of the Hurricane Fault in southwestern
685 UtahSpecial Study 119, Utah Geological Society, 81, 2007.

Marty, B., and Jambon, A.: C/$_3$He in volatile fluxes from the solid Earth: Implications for carbon geodynamics, Earth and Planetary Science Letters, 70, 196-206, 1987.

McCrea, J. M.: On the isotope chemistry of carbonates and a paleotemperature scale, The Journal of Chemical Physics, 18, 849-857, 1950.

690   Mozafari, M., Swennen, R., Balsamo, F., Clemenzi, L., Storti, F., El Desouky, H., Vanhaecke, F., Tueckmantel, C., Solum, J., and Taberner, C.: Paleofluid Evolution In Fault-Damage Zones: Evidence From Fault–Fold Interaction Events In the Jabal Qusaybah Anticline (Adam Foothills, North Oman), Journal of Sedimentary Research, 85, 1525-1551, 2015.

Mozley, P. S., and Goodwin, L. B.: Patterns of cementation along a Cenozoic normal fault:A record of paleoflow orientations, Geology, 23, 539-542, 1995.

695   Nelson, S. T., and Tingey, D. G.: Time-transgressive and extension-related basaltic volcanism in southwest Utah and vicinity, Geological Society of America Bulletin, 109, 1249-1265, 1997.

Nelson, S. T., Mayo, A. L., Gilfillan, S., Dutson, S. J., Harris, R. A., Shipton, Z. K., and Tingey, D. G.: Enhanced fracture permeability and accompanying fluid flow in the footwall of a normal fault: The Hurricane fault at Pah Tempe hot springs, Washington County, Utah, Geological Society of America Bulletin, 109, 1249-1265, 2009.

700   Newell, D. L., Jessup, M. J., Cottle, J. M., Hilton, D., Sharp, Z., and Fischer, T.: Aqueous and isotope geochemistry of mineral springs along the southern margin of the Tibetan plateau: Implications for fluid sources and regional degassing of CO_2, Geochemistry, Geophysics, and Geosystems, 9, Q08014, doi:08010.01029/02008GC002021, 2008.

Newell, D. L., Jessup, M. J., Hilton, D. R., Shaw, C. A., and Hughes, C. A.: Mantle-derived helium in hot springs of the Cordillera Blanca, Peru: Implications for mantle-to-crust fluid transfer in a flat-slab subduction setting, Chemical Geology, 417, 200 - 209,
705   2015.

Newell, D. L., and Koger, J. M.: Calcite vein C and O stable isotope values, fluid inclusion microthermometry, and U-Th dates from the Hurricane Fault zone, Utah and Arizona, USA., Interdisciplinary Earth Data Alliance (IEDA), 2020.

Nuriel, P., Rosenbaum, G., Uysal, T. I., Zhoa, J. X., Golding, S. D., Weinberger, R., Karabacak, V., and Avni, Y.: Formation of fault-related calcite precipitates and their implications for dating fault activity in the East Anatolian and Dead Sea fault zones,
710   Geological Society, London, Special Publications, 359, 229-248, 2011.

Nuriel, P., Weinberger, R., Rosenbaum, G., Golding, S. D., Zhao, J., Tonguc Uysal, I., Bar-Matthews, M., and Gross, M. R.: Timing and mechanism of late-Pleistocene calcite vein formation across the Dead Sea Fault Zone, northern Israel, Journal of Structural Geology, 36, 43-54, 2012.

O'Neil, J. R., Adami, L. H., and Epstein, S.: Revised value for the $_{18}$O fractionation between CO_2 and H_2O at 25°C, J. Res. US
715   Geol. Surv, 3, 623-624, 1975.

O'Neil, R. R., Clayton, R. N., and Mayeda, T. K.: Oxygen isotope fractionation in divalent metal carbonates, Journal of Chemical Physics, 51, 5547-5558, 1969.

Pearthree, P. A., Menges, C. M., and Mayer, L.: Distribution, recurrence, and possible tectonic implications of late Quaternary faulting in ArizonaArizona Geological Survey OFR-83-20, 1983.

720   Quigley, M. C., Karlstrom, K., and Kelley, S.: Influence of Proterozoic and Laramide structures on the Miocene extensional strain field, SE Nevada, Geological Society of America Abstracts with Programs, 2002, 9,

Quirk, B. J., Fernandez, D. P., Mackey, G. N., Armstrong, A., and Moore, J. R.: Speleothem and glacier records of Late Pleistocene-Early Holocene climate change in the Western North American Interior, Journal of Quaternary Science, in review.

Ramsay, J. G.: The crack-seal mechanism of rock deformation, Nature, 284, 135-139, 1980.

725   Rowley, P., Williams, V., Vice, G., Maxwell, D., Hacker, D., Snee, L., and Mackin, J.: Interim geologic map of the Cedar City 30' x 60' quadrangle, Iron and Washington Counties, Utah, Utah Geological Society, 2008.

Sharp, Z. D.: Principles of Stable Isotope Geochemistry, Pearson/Prentice Hall, Upper Saddle River, N.J., 344 pp., 2007.

Sherwood Lollar, B., Ballentine, C. J., and O'Nions, R. K.: The fate of mantle-derived carbon in a continental sedimentary basin: Integration of C/He relationships and stable isotope signatures, Geochimica et Cosmochimica Acta, 61, 2295-2307, 1997.

730 Shipton, Z. K., Evans, J. P., Kirschner, D., Kolesar, P. T., Williams, A. P., and Heath, J.: Analysis of CO2 leakage through 'low-permeability'faults from natural reservoirs in the Colorado Plateau, east-central Utah, Geological Society, London, Special Publications, 233, 43-58, 2004.

Sibson, R. H.: Crustal stress, faulting and fluid flow, Geological Society, London, Special Publications, 78, 69-84, 1994.

Sibson, R. H.: Structural permeability of fluid-driven fault-fracture meshes, Journal of Structural Geology, 18, 1031-1042, 1996.

735 Smith, R. B., Nagy, W. C., Julander, K., Viveiros, J. J., Barker, C. A., and Gants, D. G.: Geophysical and tectonic framework of the eastern Basin and Range-Colorado Plateau-Rocky Mountain transition, in: Geophysical Framework of the Continental United States, Geol. Soc. Am. Mem Boulder, CO, 205-233, 1989.

Stenner, H. D., and Pearthree, P. A.: Paleoseismology of the southern Anderson Junction section of the Hurricane Fault, northwestern Arizona and southwestern Utah, Arizona Geological Survery, Tucson, AZArizona Geological Survey Open-File
740 Report 99-8, 1999.

Stewart, M. E., and Taylor, W. J.: Structural analysis and fault segment boundary identification along the Hurricane fault in southwestern Utah, Journal of Structural Geology, 18, 1017-1029, 1996.

Swanson, E. M., Wernicke, B. P., Eiler, J. M., and Losh, S.: Temperatures and fluids on faults based on carbonate clumped–isotope thermometry, American Journal of Science, 312, 1-21, 2012.

745 Tuccillo, M. E., Cozzarelli, I. M., and Herman, J. S.: Iron reduction in the sediments of a hydrocarbon-contaminated aquifer, Applied Geochemistry, 14, 655-667, 1999.

USGS: ANSS Comprehensive Earthquake Catalog, accessed April 20, 2020 athttps://earthquake.usgs.gov/earthquakes/search/, 2020.

Williams, R. T., Goodwin, L. B., Mozley, P. S., Beard, B. L., and Johnson, C. M.: Tectonic controls on fault zone flow pathways
750 in the Rio Grande rift, New Mexico, USA, Geology, 43, 723-726, 2015.

Williams, R. T., Goodwin, L. B., and Mozley, P. S.: Diagenetic controls on the evolution of fault-zone architecture and permeability structure: Implications for episoldicity of fault-zone fluid transport in extensional basins, Geological Society of America Bulletin, 129, 464-478, 2017a.

Williams, R. T., Goodwin, L. B., Sharp, W. D., and Mozley, P. S.: Reading a 400,000-year record of earthquake frequency for an
755 intraplate fault, Proceedings of the National Academy of Sciences, 114, 4893-4898, 2017b.

Williams, R. T., Beard, B. L., Goodwin, L. B., Sharp, W. D., Johnson, C. M., and Mozley, P. S.: Radiogenic isotopes record a 'drop in a bucket'–A fingerprint of multi-kilometer-scale fluid pathways inferred to drive fault-valve behavior, Journal of Structural Geology, 125, 262-269, 2019.

Yonkee, W. A., and Weil, A. B.: Tectonic evolution of the Sevier and Laramide belts within the North American Cordillera orogenic
760 system, Earth-Science Reviews, 150, 531-593, 2015.

Zandt, G., Myers, S. C., and Wallace, T. C.: Crust and mantle structure across the Basin and Range-Colorado Plateau boundary at 37°N latitude and implications for Cenozoic extensional mechanism, Journal of Geophysical Research: Solid Earth, 100, 10529-10548, 1995.